

Instantaneous phase-shift Fizeau interferometer utilizing a synchronous frequency shift mechanism

Brad Kimbrough, Eric Frey, James Millerd

4D Technology Corporation, 3280 E. Hemisphere Loop, Suite 146, Tucson, AZ 85706
(520) 294-5600, (520) 294-5601 Fax, brad.kimbrough@4dtechnology.com

An on-axis, vibration insensitive, polarization Fizeau interferometer is realized through the use of a pixelated polarization mask spatial carrier phase shifting technique in conjunction with a high coherence source and a polarization frequency shift device. In this arrangement, differential motion between the test and reference surfaces, in conjunction with the polarization frequency shift device, is used to effectively separate the orthogonally polarized test and reference beam components for interference. With both the test and the reference beams on-axis, the common path cancellation advantages of the Fizeau interferometer are maintained. Additionally, the use of a high coherence source eliminates the need to path match the test and reference arms of the interferometer. Using a 1 mW HeNe source, the optimum camera shutter speed, used when measuring a 4% reflector, was 250 usec, resulting in significantly reduced vibration sensitivity. Experimental results show the performance of this new interferometer to be within the specifications of commercial phase shifting interferometers.

INTRODUCTION

Determination of the spatial variations of optical phase is of primary importance in the fields of optical testing and metrology, optical information processing, and adaptive optics. There exist several techniques for the encoding of spatial phase modulation in fringe patterns and the subsequent analysis of these fringe patterns for a quantitative determination of phase.¹ The two primary groups of fringe pattern analysis techniques are: Temporal phase measurement, sometimes known as the phase shifting method, and spatial phase measurement which is also called the spatial carrier method.

Temporal phase measurement is a well-established method for measuring optical wavefront phase². In this technique, three or more interferogram intensity profiles are recorded. For each recording, there is a different relative phase between the test and reference beams. The phase distribution of the test wavefront is then calculated using the recorded interferogram intensities. DeGroot, et. al. demonstrated the measurement of multiple surfaces within a cavity using wavelength tuning and temporal phase-shifting³.

Spatial phase measurement utilizes a single interferogram to extract phase information.⁴ In this technique, a spatial carrier, typically in the form of high frequency tilt fringes, is applied to the interferogram. The intensity profile of the modulated spatial carrier interferogram is recorded and then analyzed to determine the phase. The primary advantage of the spatial phase measurement technique over temporal phase measurement is that only one image is required, allowing acquisition times several orders of magnitude smaller than in temporal phase shifting. Rapid acquisition offers both significant vibration immunity, and the ability to measure dynamic events.

A novel approach to spatial phase measurement has been developed by 4D Technology Corporation called the *pixelated mask spatial carrier method*.⁵ In this technique, the relative phase between carrier and test wavefront is modified on a pixel-by-pixel basis by a micro-polarizer phase shifting array placed just prior to detection. This technique requires that the test and reference beams be orthogonally polarized.

This method has been successfully implemented in a Twyman-Green interferometer that uses a polarizing beam splitter to separate the source wavefront into orthogonally polarized test and reference beams.

Another interferometer configuration, the Fizeau interferometer, is often preferable for several reasons. In the Fizeau configuration, the test and reference beams are not separated as in the Twyman-Green, but travel along a common-path to the reference surface. Due to this almost common path arrangement, the Fizeau interferometer is substantially simpler in design, and only the reference surface must be produced with a high optical precision.

Unfortunately, the main advantage of the Fizeau configuration—the common path arrangement—is also the main drawback for implementing a polarization Fizeau interferometer, as it proves difficult to separate the two polarizations for interference.

One solution to this problem is to introduce an angle between reference and test beams. The angle can be used to generate a spatial carrier pattern directly on the sensor⁶, or filtered for polarization using a polarizing prism and then recombined.⁷ The major drawback with this technique is that with the tilted reference surface, the returning test and reference beams no longer follow a common path, resulting in so-called retrace errors in the measurement, which negates the common-path nature of the Fizeau. For planar reference and test optics it is possible to design the interferometer to have reasonably low retrace errors; however, the use of transmission spheres introduces substantial retrace errors. In addition, there is a direct tradeoff between the spatial resolution of the measurement and the retrace errors. The use of small tilts, on the order of a few dozen fringes produces a small retrace error ($<1/10^{\text{th}}$ wave) but the data must be filtered to avoid harmonics (either optically or in software) leaving only very low spatial frequencies. The use of higher angles allows the filter bandwidth to be increased but the retrace error increases dramatically. Calibration at large tilts is difficult because of the need to induce the exact amount of tilt between measurements and the attendant error introduced from subtracting large aberrations to calculate small values.

Küchel proposed the use of a low temporal coherence source and an optical delay-line that splits the source beam into two orthogonally polarized components and allows a controllable phase difference between the two beams.⁸ In a previous paper, we reported on the combination of Küchel's delay-line Fizeau configuration with the pixelated-mask instantaneous phase sensor, resulting in an on-axis, vibration insensitive Fizeau interferometer.⁹ In addition to the benefits of on-axis operation and vibration insensitivity, use of a low temporal coherence source allows specific surfaces within the measurement cavity to be isolated for interference. Surface isolation makes remote cavity measurements and measurements of thin lenses or plates possible.

While the short-coherence method works well for many applications, it is less well suited for test set-ups with very long cavity lengths, for example large telescopes or beam trains, or in situations where multiple surface reflections are not present. Additionally, measurement cavity lengths are restricted by the maximum OPD obtainable with the interferometer's internal path matching mechanism.

In order to provide a high quality, general lab instrument that can easily be configured and used over very long path lengths, we have developed the instrument described in this paper. It has the advantages of an on-axis Fizeau design together with vibration insensitive measurement capability and long temporal coherence. The Fizeau interferometer is realized through the use of a pixelated polarization mask spatial carrier phase shifting technique, in conjunction with a polarization frequency shifting device. In this arrangement, differential motion between the test and reference surfaces, in conjunction with the polarization frequency shift device, is used to effectively separate out the orthogonally polarized test and reference beam components for interference. With both the test and the reference beams on-axis, the common path cancellation advantages of the Fizeau interferometer are maintained. Additionally, the use of a high coherence source eliminates the need to path match the test and reference arms of the interferometer. In this paper we present the theory of operation of the instrument and some measurement results that have been obtained.

THEORY OF OPERATION

The basic layout of the synchronous frequency shifting Fizeau interferometer is shown in figure 1. This system is composed of three major sections: (1) A high coherence source, (2) A polarization frequency shifting device; and (3) A Fizeau interferometer with a pixelated mask sensor.

The source used in our experiments was a 1mW stabilized HeNe laser. However, the only requirement is that the laser source coherence length be at least as large as the Fizeau cavity being measured.

The polarization frequency shift device is essentially a polarization Twyman-Green interferometer. It consists of a half wave plate, HWP, a polarizing beam splitter, PBS, two quarter wave plates, QWP, a fixed retro reflector, and moving retro reflector. The polarization frequency shifting device splits the source beam into two orthogonally polarized components and applies a controllable frequency shift to one polarization component of the beam relative to the other orthogonally polarized component. This frequency shift is obtained by rapidly translating the moving retro reflector in a direction parallel to the beam. The two beams are then recombined and spatially filtered.

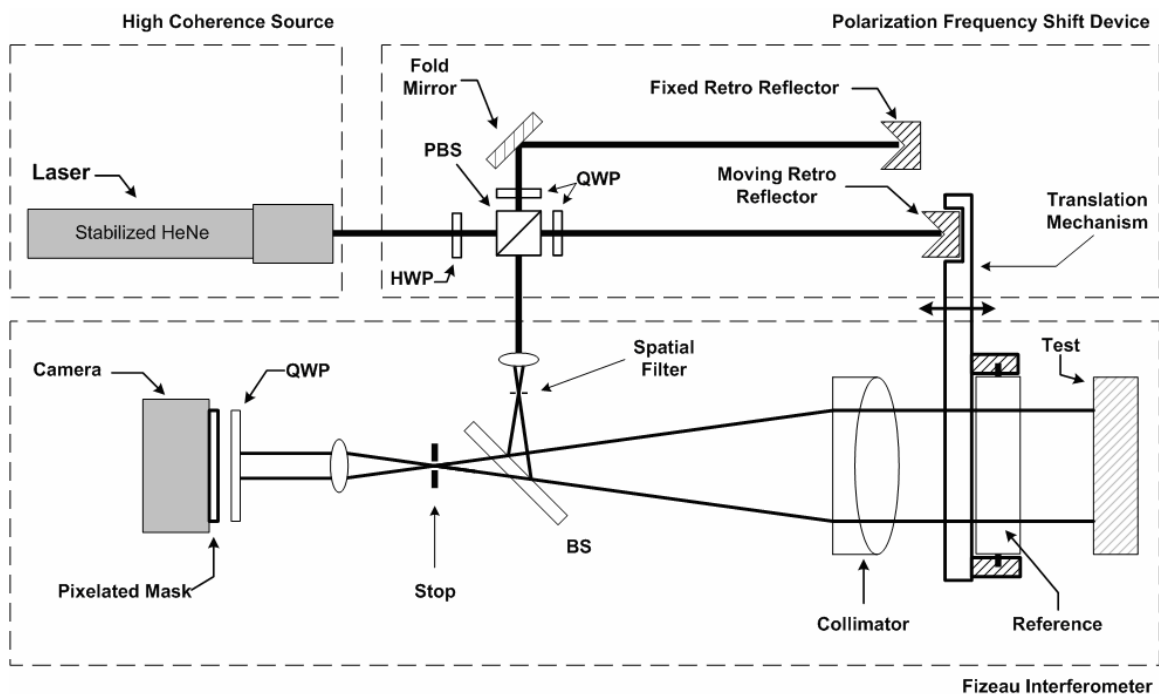


Figure 1: Instantaneous phase-shift Fizeau interferometer utilizing a synchronous frequency shifting mechanism.

The combined beam is then launched into a standard Fizeau cavity consisting of a reference and a test optic. It is convenient to think of this input beam as being composed of two separate but overlapping beams, the s -polarized beam and the p -polarized beam. The s -polarized beam originated in the moving leg and is frequency shifted relative to the p -polarized beam which originated in the fixed leg. The half wave plate just in front of the laser source is used to adjust the intensity ratio between the two beams. Maximum visibility is obtained when the intensities of the s and p components are matched, regardless of the test and reference mirror reflectivities.⁹

Both the s and p -polarized beams illuminate and are reflected by the test and reference surfaces. The reference surface is translated in a direction substantially parallel to the incident optical beam, such that the reflected beams are imparted with a frequency shift equal in magnitude with the polarization frequency shift device. The returning beams are imaged onto the pixelated mask sensor. The quarter wave plate, QWP, just prior to the pixelated mask is used to convert the

linearly polarized test and reference beams into right and left circular polarizations as is necessary for the operation of the pixelated mask sensor.⁵ Alternatively, the quarter wave plate can be introduced just prior to the spatial filter to produce orthogonal circularly polarization between the two beams.

There are essentially 4 beams incident upon the pixelated mask sensor: s and p -polarized test surface reflected beams, and s and p -polarized reference surface reflected beams. For the pixelated mask sensor, the test and reference beams must be orthogonally polarized.

In this case, each of the 6 possible beam combinations produces an interference pattern at the camera. However, there is a relative frequency shift between the beams making up each pair in all but one of the beam combinations. In other words, the fringes from all but one of the beam combinations are moving. The stationary beam combination is composed of the s -polarized beam from the test surface and the p -polarized beam from the reference surface. The frequency shift imparted by the moving retro reflector and the reference surface is selected to produce at least one full cycle of phase shift during the integration time of the camera. Therefore, the moving fringe combinations will be highly attenuated, and the contrast of the stationary fringe combination will remain high. Thus, the system functions as a single shot, polarization phase-shift interferometer with both the reference and test beam remaining on axis.

MATHEMATICAL TREATMENT

A better understanding of the operation of the synchronous frequency shifting Fizeau interferometer may be obtained through a more rigorous analysis of its operation. The beam leaving the polarization frequency shifting device can be represented as follows:

$$\mathbf{E}(\mathbf{t}) = \begin{pmatrix} \varepsilon_p \\ \varepsilon_s e^{i\omega_c t} \end{pmatrix} \quad (1)$$

where ε_p and ε_s are the p -polarization and the s -polarization electric field components of the beam, and ω_c is the frequency shift due to the moving reflector. Assuming the moving reflector velocity, v_c is constant, ω_c is given by:

$$\omega_c = 4\pi v_c / \lambda \quad (2)$$

Following reflection from the test and reference surfaces, the electric field incident upon the QWP at the camera is given by:

$$\mathbf{E}(\mathbf{t}) = \begin{pmatrix} \varepsilon_{r_p} e^{i(\omega_r t + \theta_r)} + \varepsilon_{t_p} e^{i\theta_t} \\ \varepsilon_{r_s} e^{i((\omega_r + \omega_c)t + \theta_r)} + \varepsilon_{t_s} e^{i(\omega_c t + \theta_t)} \end{pmatrix} \quad (3)$$

where ε_{r_p} and ε_{t_p} are the p -polarization components that have reflected off of the reference and test surfaces respectively, and ε_{r_s} and ε_{t_s} are the corresponding s -polarization components. θ_r and θ_t represent the wavefront phase resulting from reflection off of the reference and test surfaces respectively. Finally, ω_c is the frequency shift due to the moving reference surface which is given by equation 2 with v_c replaced by v_r , the reference surface velocity.

Prior to reaching the detector, the light must pass through a QWP oriented at 45 degrees to the horizontal and through the pixelated polarization mask. This mask is made up of discrete polarizers having dimensions equal to the detector pixels with alternating orientations of 0, 45, 90, and 135 degrees. Using Jones calculus, the electric field at the detector is given by:

$$\mathbf{E}(\alpha, \mathbf{t}) = P(\alpha) \text{QWP}_{\frac{\pi}{4}} \begin{pmatrix} \varepsilon_{r_p} e^{i(\omega_r t + \theta_r)} + \varepsilon_{t_p} e^{i\theta_t} \\ \varepsilon_{r_s} e^{i((\omega_r + \omega_c)t + \theta_r)} + \varepsilon_{t_s} e^{i(\omega_c t + \theta_t)} \end{pmatrix} \quad (4)$$

where $P(\alpha)$ is the Jones matrix for a polarizer with an orientation of α , and $QWP_{\pi/4}$ is the Jones matrix for a QWP with its fast axis oriented at an angle of $\pi/4$ with respect to the horizontal. The intensity at the camera is found by multiplying equation 4 by its complex conjugate giving:

$$I(\alpha, t) = C/2 \left(\begin{aligned} & (\epsilon r_p^2 + \epsilon t_s^2 + 2 \epsilon r_p \epsilon t_s \sin[(\theta_t - \theta_r) + (w_r - w_c) t + 2\alpha]) \\ & + (\epsilon r_s^2 + \epsilon t_p^2 - 2 \epsilon r_s \epsilon t_p \sin[(\theta_t - \theta_r) + (w_r + w_c) t - 2\alpha]) \\ & + 2 \epsilon r_s \epsilon t_s \cos[(\theta_t - \theta_r) + w_r t] \\ & + 2 \epsilon r_p \epsilon t_p \cos[(\theta_t - \theta_r) + w_r t] \\ & + 2 \epsilon r_s \epsilon r_p \sin[w_c t + 2\alpha] \\ & + 2 \epsilon t_p \epsilon t_s \sin[w_c t + 2\alpha] \end{aligned} \right) \quad (5)$$

where C is a constant of conversion between the electric field squared and the intensity. Expressing the electric fields in terms of intensity gives the general expression for the intensity at the detector behind a pixelated mask polarizer with and orientation of α .

$$I(\alpha, t) = \begin{aligned} & \frac{1}{2} \left(I r_p^2 + I t_s^2 + 2 \sqrt{I r_p I t_s} \sin[(\theta_t - \theta_r) + (w_r - w_c) t + 2\alpha] \right) \\ & + \frac{1}{2} \left(I r_s^2 + I t_p^2 - 2 \sqrt{I r_s I t_p} \sin[(\theta_t - \theta_r) + (w_r + w_c) t - 2\alpha] \right) \\ & + \sqrt{I r_s I t_s} \cos[(\theta_t - \theta_r) + w_r t] \\ & + \sqrt{I r_p I t_p} \cos[(\theta_t - \theta_r) + w_r t] \\ & + \sqrt{I r_s I r_p} \sin[w_c t + 2\alpha] \\ & + \sqrt{I t_p I t_s} \sin[w_c t + 2\alpha] \end{aligned} \quad (6)$$

Notice that there are six interference terms in equation 6 above, the first interference term is what we want to measure, and is the interference of the p -polarization off of the reference surface, and the s -polarization off of the test. The second line represents the interference of the s -polarization off of the reference and the p -polarization off of the test. The third and fourth terms represent the interference of the s -polarization off of the test and reference surfaces, and of the p -polarizations off of the test and reference surfaces. These two terms have no α dependence and will therefore not be phase shifted by the pixelated mask sensor. The final two terms represent the interference of the s and p -polarizations off of the reference surface and off of the test surface respectively. The final interference terms represent only piston and have no surface dependence. If we make the frequency shift due to the moving retro-reflector equal to that caused by the moving reference surface we can set $w_r = w_c$, and the time dependent component in the first interference term goes to zero. In order to clean things up a bit, let $\theta_t - \theta_r = \Delta\theta$. Equation (6) then becomes:

$$\begin{aligned}
I(\alpha, t) = & \\
& \frac{1}{2} \left(I_{r_p}^2 + I_{t_s}^2 + 2 \sqrt{I_{r_p} I_{t_s}} \sin[\Delta\theta + 2\alpha] \right) \\
& + \frac{1}{2} \left(I_{r_s}^2 + I_{t_p}^2 - 2 \sqrt{I_{r_s} I_{t_p}} \sin[\Delta\theta + 2\omega_c t - 2\alpha] \right) \\
& + \sqrt{I_{r_s} I_{t_s}} \cos[\Delta\theta + \omega_c t] \\
& + \sqrt{I_{r_p} I_{t_p}} \cos[\Delta\theta + \omega_c t] \\
& + \sqrt{I_{r_s} I_{r_p}} \sin[\omega_c t + 2\alpha] \\
& + \sqrt{I_{t_p} I_{t_s}} \sin[\omega_c t + 2\alpha]
\end{aligned} \tag{7}$$

The camera signal is found by integrating equation 7 for the camera exposure time. The results of this integration can be represented as follows:

$$\begin{aligned}
I(\alpha, T) \propto & \\
& \frac{1}{2} \left(I_{r_p}^2 + I_{t_s}^2 + I_{r_s}^2 + I_{t_p}^2 + 2 \sqrt{I_{r_p} I_{t_s}} \sin[\Delta\theta + 2\alpha] \right) \\
& + \frac{2 \sin\left[\frac{2T\omega_c}{2}\right]}{2T\omega_c} \sqrt{I_{r_s} I_{t_p}} \sin[2\alpha - \Delta\theta] \\
& + \frac{2 \sin\left[\frac{T\omega_c}{2}\right]}{T\omega_c} \left(\sqrt{I_{r_s} I_{t_s}} \cos[\Delta\theta] + \sqrt{I_{r_p} I_{t_p}} \cos[\Delta\theta] \right. \\
& \quad \left. + \sqrt{I_{r_s} I_{r_p}} \sin[2\alpha] + \sqrt{I_{t_p} I_{t_s}} \sin[2\alpha] \right)
\end{aligned} \tag{8}$$

where T is equal to the camera integration time. Due to the time integration, all of the interference terms except the first are multiplied by an attenuating factor. A plot of the attenuation factors as a function of the integration time is shown in figure 2.

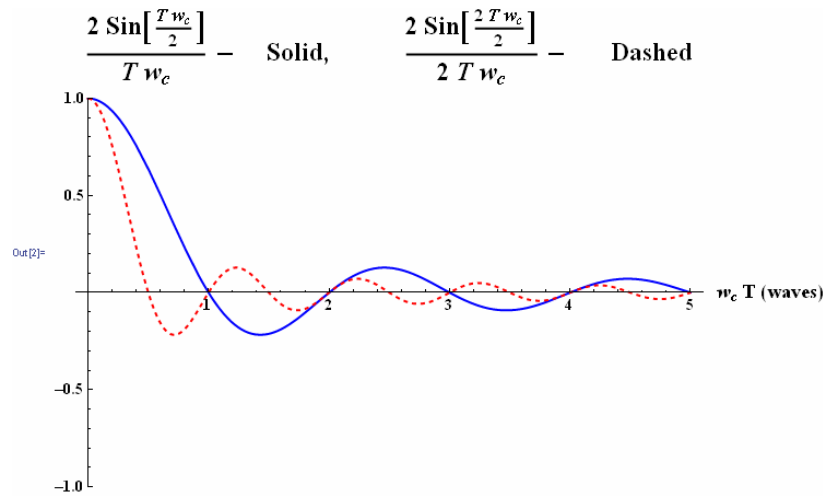


Figure 2: Plot of attenuation factors from equation 8 as a function of frequency shift and camera integration time. Both attenuation factors are zero when the total phase change during integration is an integer multiple of 2π .

Notice that when the total phase change during integration is a multiple of 2π , both factors become zero. At these points, equation 8 reduces to:

$$I(\alpha, T) \propto \frac{1}{2} \left(I_{r_p}^2 + I_{t_s}^2 + I_{r_s}^2 + I_{t_p}^2 + 2 \sqrt{I_{r_p} I_{t_s}} \sin[\Delta\theta + 2\alpha] \right) \quad (9)$$

Equation 9 represents the interference pattern between the p -polarized light reflecting off of the reference surface and the s -polarized light reflecting off of the test surface. The DC terms $I_{r_s}^2$ and $I_{t_p}^2$ provide additional background light and limit the maximum fringe visibility to 50%; however, on a 10 bit camera properly biased, this still results in 8-9 bits of interference signal. As stated earlier, the polarization angle at the pixelated mask alternates between 0, 45, 90, and 135 degrees. This creates the necessary phase shift of 0, 90, 180, and 270 degrees between interferograms, and allows the phase difference between the test and reference surfaces, $\Delta\theta$ to be determined.

Reference eight provides a detailed analysis of the fringe visibility resulting from a fringe pattern described by equation 9. The visibility can be shown to be given by:

$$\text{visibility} = \left(\frac{\sqrt{I_s I_p}}{I_s + I_p} \right) \frac{(1 - R_r) (1 - R_t) \sqrt{R_r R_t}}{(1 - R_r) R_t + (1 - R_t) R_r} \quad (10)$$

where R_r and R_t are the reference and test surface reflectivity's, and I_s and I_p are the s and p -polarized light intensities entering the interferometer. It can also be shown that the maximum fringe contrast of 50% is obtained when I_s and I_p are matched, regardless of the test and reference surface reflectivity's.

SYSTEM DESIGN

An on-axis vibration insensitive polarization Fizeau interferometer was built based on the layout shown in figure 1. The system was built with a stabilized 1mW HeNe laser, a 1 Mpixel CCD camera, and a 4 inch output aperture. The translation mechanism for the reference surface and moving retro reflector required a careful design. The reference flat mounting needed to be stiff enough to withstand the forces generated during accelerations up to the measurement velocity, but at the same time not cause significant stress in the glass and distort the reference surface. It also needed to damp any vibration caused by the impulse of the transmission optic's rapid motion profile. The translation mechanism utilizes three low voltage piezo actuator stacks, each having its own driver. Independent piezo drivers allow adjustment of the translation to ensure straightness under different load conditions, such as the use of different reference spheres or flats. The translation velocity was chosen to produce 4 waves of OPD change for a 0.5 msec camera exposure. This translates into a movement of about 2.52 $\mu\text{m} / \text{msec}$. The piezo movement profile is shown below in figure 3. Camera exposure is centered at the inflection of the outward motion where acceleration passes through zero. Following the measurement, the flat is returned to its starting position with a gentler motion profile. This motion profile is repeated at a rate of up to 20 times per second allowing near standard video rate data collection.

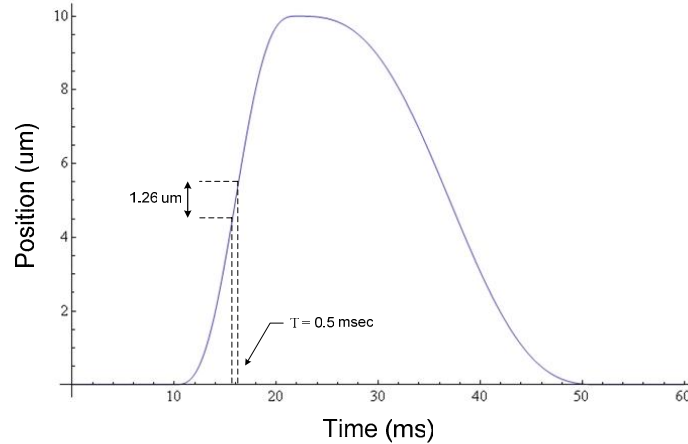


Figure 3: Typical motion profile of the reference flat. The camera exposure is centered about the inflection point of the outward motion. In this example, the exposure time is set to 0.5 msec during which time the flat moves 1.26 um resulting in 4 waves of OPD change.

Timing and Balancing

Optimum system performance is obtained when the extraneous fringes are fully attenuated, and at the same time, the desired fringe contrast is maximized. As discussed above, full attenuation of the extraneous fringes will only be achieved when the reference flat and retro reflector are translated integer multiples of a half wavelength as discussed above. The appropriate timing settings are determined by monitoring the phase print-through errors while adjusting the timing parameters.

In order to maintain the contrast of the desired fringes, the reference flat motion must match the retro reflector motion for all points on the flat. This means that the flat must translate without tilting. Once the timing has been set properly, piezo drive balance parameters are changed while monitoring the fringe contrast. The balance position is set at the point of maximum fringe contrast. The results of a balancing scan are shown below in figure 4. Fringe visibility is plotted as a function of drive signal for piezo one (X) and piezo three (Y).

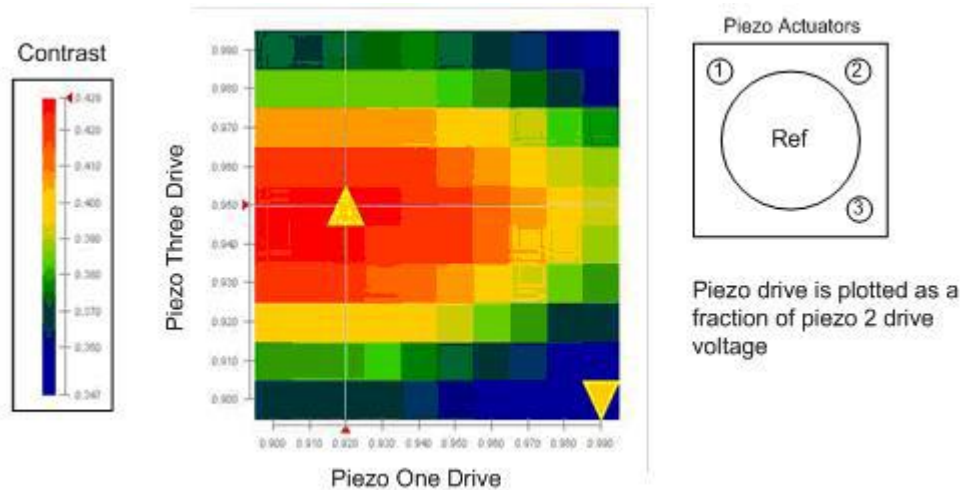


Figure 4: Fringe visibility as a function of piezo drive signal. The drive signal for piezo one (X) and for piezo three (Y) are given as a fraction of piezo two drive.

MEASUREMENT RESULTS

The synchronous phase shifting Fizeau interferometer that was built can be operated in both dynamic mode as discussed above, and in standard temporal phase shifting mode. Temporal phase shifting mode is conducted by blocking the *s*-polarized beam, and phase shifting the flat by fractions of a wavelength, typically $\lambda/4$, between measurements. Since temporal mode requires the acquisition of at least four frames of data at the standard video rate of 30 fps, total acquisition time is at least 120 ms. By comparison, the dynamic measurements were taken with an integration time of about 250 usec. Due to the relatively long acquisition time, the temporal measurements must be conducted on a vibration isolated surface. Figure 5 below show the results of both temporal and dynamic measurements on a 6 inch return flat. The reflectivity of the flat was 4%. Each measurement is the average of 16 individual measurements. The interferometer and flat were placed on a floating table for the temporal measurements. For the dynamic measurements, the vibration isolation on the table was removed. In our laboratory environment, temporal measurements were not possible if the table was not floated. As can be seen, the dynamic measurement is very close to the temporal measurement result. The flat was specified to be 1/20 wave over 6 inches of clear aperture. The measurement clear aperture was 4 inches. The temporal measurement has a peak-to-valley and RMS of 0.0395 and 0.0008 waves respectively. For the dynamic measurement, the peak-to-valley and RMS were 0.0382 and 0.0008 waves respectively.

Measurement of a Flat

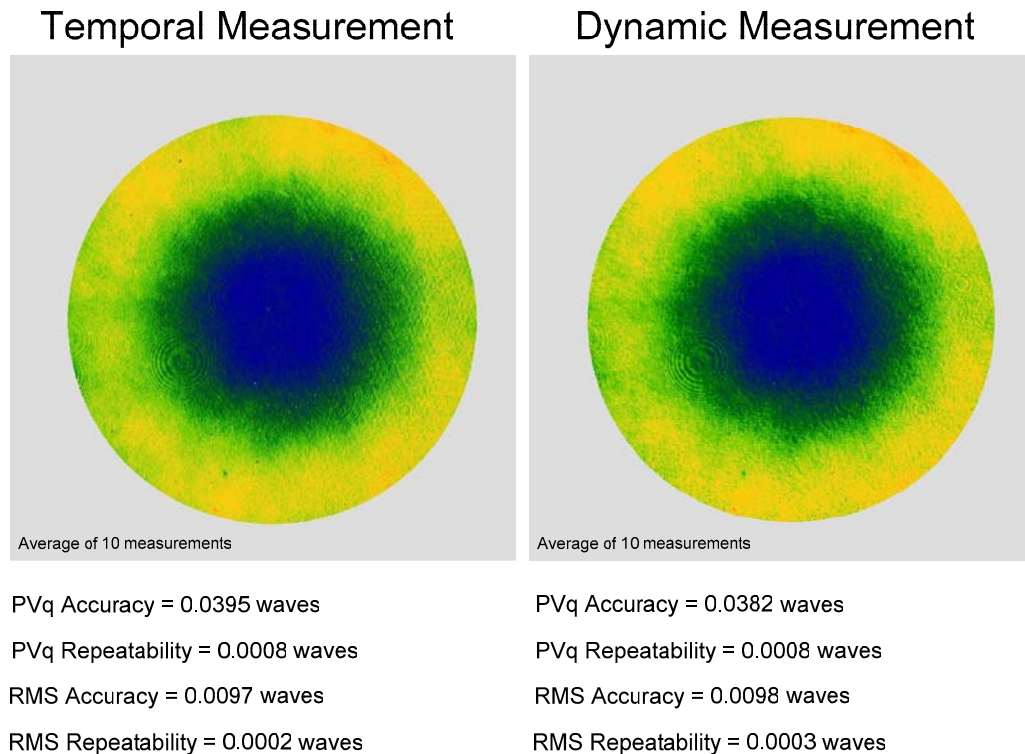


Figure 5: Measurement of a flat in both temporal and dynamic mode. Each measurement is the average of 10 individual measurements. Temporal measurements were conducted on a floating table. For the dynamic measurements, the float was removed.

One of the primary advantages of an on-axis dynamic Fizeau interferometer over dynamic systems that utilize a tilted beam arrangement is that a transmission sphere can be used without introducing several waves of retrace error. Measurements of the convex surface of a plano-convex lens using an *f* 3.5 reference sphere were conducted. The reference sphere was specified at 1/10 wave. The lens had a diameter of 50.4mm, a focal length of 200 mm, and was

uncoated. Measurement results are shown in figure 6. The noise peak in the center is due to a stray reflection off of the back planar surface of the lens. The temporal measurement has a peak-to-valley and RMS of 0.1294 and 0.0263 waves respectively. For the dynamic measurement, the peak-to-valley and RMS were 0.1303 and 0.0260 waves respectively.

Measurement of a Concave Surface

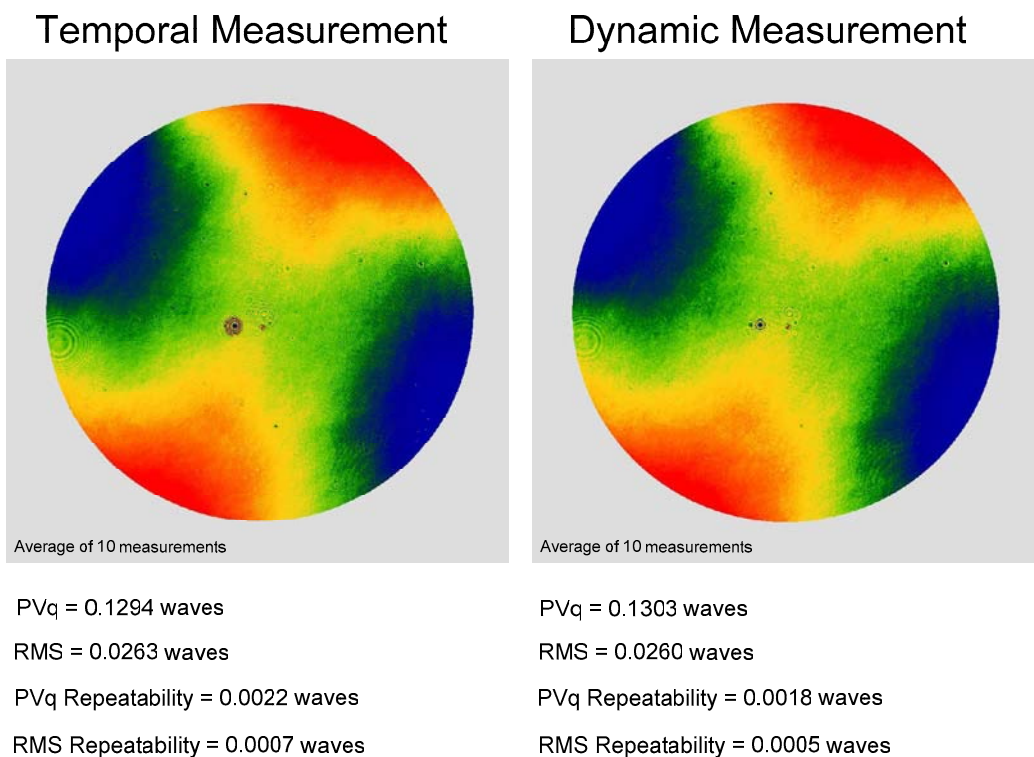


Figure 6: Measurement of the convex surface of a plano-convex lens. The result shown is the average of 10 individual measurements. Temporal measurements were conducted on a floating table. For the dynamic measurements, the float was removed.

CONCLUSION

An on-axis, vibration insensitive, polarization Fizeau interferometer is realized through the use of a pixelated polarization mask spatial carrier phase shifting technique in conjunction with a high coherence source and a polarization frequency shift device. In this arrangement, differential motion between the test and reference surfaces, in conjunction with the polarization frequency shift device, is used to effectively separate out the orthogonally polarized test and reference beam components for interference. To facilitate understanding of the mechanism of operation, a simple four beam interference model was derived, and the specific motion and timing requirements discussed. The results of measurements on a flat and a sphere were given. Each of these measurements was well within the specification of the parts measured, demonstrating that with both the test and the reference beams on-axis, the common path cancellation advantages of the Fizeau interferometer are maintained. Additionally, the use of a high coherence source eliminates the need to path match the test and reference arms of the interferometer. Using a 1 mW HeNe source, the maximum camera shutter speed, used when measuring a 4% reflector, was 250 usec, resulting in significantly reduced vibration sensitivity. Experimental results show the performance of this new interferometer to be within the specifications of commercial phase shifting interferometers.

REFERENCES

1. D. Malacara, M. Servin, and Z. Malacara, "Interferogram analysis for optical testing," (Marcel Dekker, New York, 1998).
2. D. Malacara, *Optical Shop Testing* (Wiley, New York, 1992).
3. P. de Groot, Measurement of Transparent Plates with Wavelength-Tuned Phase-Shifting Interferometry, *Applied Optics* 39 (16), 2658-2663, June 2000.
4. R. Jozwicki, M. Kujawinska, and L. Salbut, "New contra old wavefront measurement concepts for interferometric optical testing," *Optical Engineering* 31, 422 , (1992).
5. J. E. Millerd, N. J. Brock, J. B. Hayes, M. B. North-Morris, M. Novak, and J. C. Wyant, "Pixelated phase-mask dynamic interferometer," *Proc. SPIE* 5531, 304-314, (2004).
6. Fizeau Interferometers Evaluated Using FlashPhase and Phase-Shift Fringe Analysis, E Rabinovich and B. Carr, *Photonics Spectra Magazine*, August, 2006.
7. J. E. Millerd in "Fringe 2005," edited by W. Osten, (Springer, New York, 2005), pg 640.
8. M. Küchel, "Interferometer for measuring optical phase difference," U. S. Patent 4,872,755 (1989).
9. B. Kimbrough, J. Millerd, J. Wyant, J. Hayes, "Low Coherence Vibration Insensitive Fizeau Interferometer," *Proc. SPIE* 6292, (2006).